Factors Influencing Simulated Changes in Future Arctic Cloudiness

STEPHEN J. VAVRUS

Nelson Institute Center for Climatic Research, University of Wisconsin—Madison, Madison, Wisconsin

UMA S. BHATT

Geophysical Institute, University of Alaska Fairbanks, Fairbanks, Alaska

VLADIMIR A. ALEXEEV

International Arctic Research Center, University of Alaska Fairbanks, Fairbanks, Alaska

(Manuscript received 25 August 2010, in final form 15 April 2011)

ABSTRACT

This study diagnoses the changes in Arctic clouds simulated by the Community Climate System Model version 3 (CCSM3) in a transient $2 \times CO_2$ simulation. Four experiments—one fully coupled and three with prescribed SSTs and/or sea ice cover—are used to identify the mechanisms responsible for the projected cloud changes. The target simulation uses a T42 version of the CCSM3, in which the atmosphere is coupled to a dynamical ocean with mobile sea ice. This simulation is approximated by a T42 atmosphere-only integration using CCSM3's atmospheric component [the Community Atmosphere Model version 3 (CAM3)] forced at its lower boundary with the changes in both SSTs and sea ice concentration from CCSM3's $2 \times CO_2$ run. The authors decompose the combined effect of the higher SSTs and reduced sea ice concentration on the Arctic cloud response in this experiment by running two additional CAM3 simulations: one forced with modern SSTs and the projected sea ice cover changes in CCSM3 and the other forced with modern sea ice coverage and the projected changes in SSTs in CCSM3.

The results suggest that future increases in Arctic cloudiness simulated by CCSM3 are mostly attributable to two separate processes. Low cloud gains are primarily initiated locally by enhanced evaporation within the Arctic due to reduced sea ice, whereas cloud increases at middle and high levels are mostly driven remotely via greater meridional moisture transport from lower latitudes in a more humid global atmosphere. The enhanced low cloudiness attributable to sea ice loss causes large increases in cloud radiative forcing during the coldest months and therefore promotes even greater surface warming. Because CCSM3's Arctic cloud response to greenhouse forcing is similar to other GCMs, the driving mechanisms identified here may be applicable to other models and could help to advance our understanding of likely changes in the vertical structure of polar clouds.

1. Introduction

A fundamental uncertainty in polar climate change is the relative importance of processes within high latitudes compared with remote forcing from lower latitudes. Another key unknown is how clouds will affect the Arctic's future climate trajectory. The Arctic is already undergoing a transition toward a considerably warmer and less icy future, with signs of this shift being realized unambiguously in terms of rising temperatures, declining sea ice, earlier snowmelt, and intrusions of exotic biota (Walsh et al. 2005; Overland et al. 2008; Stroeve et al. 2007; Hegseth and Sundfjord 2008). Numerous studies have also investigated recent trends in Arctic cloudiness but with conflicting findings. Satellite data from the Television and Infrared Observation Satellite (TIROS) Operational Vertical Sounder (TOVS) and the Advanced Very High Resolution Radiometer (AVHRR) showed significant Arctic cloud increases during spring and decreases during winter during the 1980s–90s (Wang and Key 2003; Schweiger 2004), whereas Comiso (2003) reported decreasing trends in all seasons over the same time period from the AVHRR dataset. Using surface observations since the early 1970s, Eastman and Warren (2010a) identify positive trends in Arctic

Corresponding author address: Stephen J. Vavrus, Nelson Institute Center for Climatic Research, 1225 W. Dayton Street, University of Wisconsin—Madison, Madison, WI 53706.
E-mail: sjvavrus@wisc.edu

DOI: 10.1175/2011JCLI4029.1

cloudiness in every season. Because of these discrepancies, the role of clouds in recent Arctic climate change remains uncertain, although calculations by Liu et al. (2009) suggest that changes in cloud cover account for a majority of the seasonal surface temperature trends between 1982 and 2004.

There is better agreement among climate models on how clouds should respond as the Arctic warms in the future. Vavrus et al. (2009) documented that GCMs participating in the Coupled Model Intercomparison Project phase 3 (CMIP3) mostly simulated a cloudier twenty-first-century Arctic, especially during autumn, resulting in a positive feedback to the warming climate. The gain in vertically integrated clouds was attributable to enhanced local evaporation associated with the loss of sea ice and was projected to be expressed as greater amounts of low clouds and high clouds, with little change in midlevel cloudiness (tripole pattern). The authors did not diagnose the cause(s) of the height dependence of the cloud changes, however, even though low clouds have considerably different radiative effects than high clouds. The simulated cloud increase accompanying a waning ice pack in the future agrees with recent observations that clouds are more prevalent when sea ice extent is anomalously low (Kay and Gettelman 2009; Eastman and Warren 2010a; Palm et al. 2010).

The primary goal of this study is to investigate more thoroughly the physical mechanisms responsible for generating the future tripole cloud response by utilizing a single GCM that is fairly representative of the CMIP3 models. Under greenhouse forcing, the Community Climate System Model (CCSM3) was found to produce Arctic cloud changes similar to the CMIP3 average, although somewhat accentuated (Vavrus et al. 2011). We use CCSM3 as the basis for our investigation by decomposing this model's future Arctic cloud response in coupled mode (interactive atmosphere, ocean, and sea ice) into the portions attributable to (i) local changes in sea ice cover and (ii) remote sea surface temperatures (SSTs) outside of polar regions. The methodology consists of running CCSM3's atmospheric component [the Community Atmosphere Model version 3 (CAM3)] with altered boundary conditions (sea ice concentration and SSTs) taken from the CCSM3 coupled simulation at the time of CO_2 doubling under transient greenhouse forcing. This technique is known as the time-slice experimental design and has been utilized by numerous investigators (e.g., Cubasch et al. 1995; Timbal et al. 1997). Several recent studies of Arctic climate have also run atmospheric models driven by prescribed sea ice and SSTs to explore the atmosphere's response to contemporary sea ice variability (Alexander et al. 2004; Bhatt et al. 2008) and projected future ice cover (Singarayer et al. 2006; Higgins and Cassano 2009; Deser et al. 2010). This research demonstrates that more open water in the Arctic is likely to cause a large increase in precipitation, significant changes in atmospheric circulation that extend into middle latitudes, and an erosion of the Arctic temperature inversion. Furthermore, warming over the Arctic Ocean caused by a retreating ice pack is likely to extend well inland and may trigger permafrost thawing (Lawrence et al. 2008; Bekryaev et al. 2010). Whereas these related studies addressed the influence of sea ice on atmospheric temperature, hydrology, and circulation, the focus of the current paper is on the role of future sea ice reductions and SST increases on clouds within the Arctic.

The present study is motivated by three overriding questions. First, what are the relative contributions to projected Arctic cloud changes from local forcing (less sea ice) and remote forcing (warmer oceans globally)? This particular question was also highlighted as an important research topic in a recent study on cloud feedbacks and polar amplification (Graversen and Wang 2009), while the general question of local versus remote influences on Arctic climate is one of the key issues being addressed by the interagency Study of Environmental Arctic Change (SEARCH). In a $2 \times CO_2$ GCM simulation, Vavrus (2004) found that cloud changes outside of polar regions affected Arctic temperature as much as those occurring within high latitudes, due to meridional energy transport feedbacks. Likewise, Alexeev et al. (2005) and Langen and Alexeev (2007) showed that a major portion of the increased meridional energy flux into polar regions under greenhouse forcing is latent heat, which could contribute to enhanced Arctic cloudiness. A second question is what processes are responsible for the tripole cloud change pattern with height in CCSM3 and the CMIP3 models, such that low clouds and high clouds should become relatively more abundant than midlevel cloudiness? Although increased *total* Arctic cloud amount has been linked to increased evaporation over the Arctic Ocean, different mechanisms such as convection and meridional moisture transport could cause the height-varying cloud response. Third, what are the radiative–climatic impacts of these height-dependent, future cloud changes in the Arctic? Because clouds in this region warm the surface except during summer, the radiative impact of cloud changes caused by a waning ice pack and a warming ocean will likely be seasonally dependent. Annually averaged, a cloudier future Arctic would probably enhance polar amplification of greenhouse warming, based on climate model simulations of an aquaplanet (Alexeev and Bates 1999; Langen and Alexeev 2004), fixed-cloud GCM experiments (Vavrus 2004), and a suite of simulations from the CMIP3 (Vavrus et al. 2009).

2. Experimental design

a. Model description

The climate model used in this study, CCSM3, is a fully coupled global climate model of the atmosphere, ocean, sea ice, and land systems (Collins et al. 2006a). Its atmospheric component, CAM3 (Collins et al. 2006b), is used here as a proxy for the behavior of the full CCSM3. The T42 (~2.8°) horizontal resolution used in these experiments is coarser than the model's standard T85 resolution, but this configuration employs the same 26 levels in its hybrid-sigma pressure coordinate system and generates similar polar cloud characteristics (Vavrus and Waliser 2008). The ocean model in the CCSM3 is the Parallel Ocean Program (POP) version 1.4.3 (Smith and Gent 2004), which includes an isopycnal transport parameterization (Gent and McWilliams 1990) and uses a nominal horizontal resolution of 1°. The dynamic–thermodynamic sea ice model—run on the same grid as the ocean component—is the Community Sea Ice Model (CSIM) (Briegleb et al. 2004), whose features include an elastic–viscous–plastic rheology (Hunke and Dukowicz 1997) and the thermodynamics of Bitz and Lipscomb (1999). The land component is the Community Land Model version 3 (CLM3) (Bonan et al. 2002), which contains 10 subsurface soil layers and computes exchanges of energy, mass, and momentum with the atmosphere. The model uses a subgrid mosaic of observed plant functional types on the same spatial grid as the atmosphere. In the atmospheric simulations with prescribed surface boundary conditions, the sea ice and ocean (and land) use the same T42 resolution as the atmosphere.

A full description of CAM3's treatment of clouds is given in Collins et al. (2006b) and Boville et al. (2006). Clouds are categorized as either convective or stratiform and are calculated separately at three levels: low (below 700 hPa), middle (700–400 hPa), and high (above 400 hPa). Condensate varies between ice and liquid as a linear function of temperature, with threshold temperatures of 233 and 263 K. The model employs a standard maximum–random cloud overlap scheme (Collins 2001) and separate parameterizations for shallow (Hack 1994) and deep (Zhang and McFarlane 1995) convection. Cloud fraction is determined diagnostically for convective and stratiform clouds, using separate calculations for deep and shallow convection. Stratiform clouds are a function of the gridbox mean relative humidity at each level and vary quadratically from a threshold humidity of 80% over land and 90% elsewhere.

b. Model performance

At both its standard T85 resolution and the coarser T42 resolution used here, CCSM3 simulates realistic amounts of Arctic clouds during summer but overestimates low cloudiness during winter, similar to many GCMs (Vavrus and Waliser 2008). Averaged over 70°–90°N the monthly total Arctic cloud cover in the model's modern control run ranges from 70% (December) to 79% (August) and is composed primarily of low clouds. CCSM3 outperforms all but 2 of 18 CMIP3 climate models in its simulation of cloud fraction at Barrow, Alaska (Walsh et al. 2008). Although CCSM3's liquid cloud condensate and thus cloud optical depth in the Arctic is known to be too high (Gorodetskaya et al. 2008; Miao and Wang 2008), its surface cloud radiative forcing (CRF) compares very favorably to measurements from the AVHRR Polar Pathfinder, outperforming all other GCMs evaluated over ice-covered regions (Karlsson and Svensson 2009). When CCSM3 is run in atmosphere-only mode (CAM3 driven with observed sea ice and SST distributions), its Arctic cloud coverage is similar to but somewhat greater than the fully coupled version, ranging from a monthly minimum of 76% to a maximum of 83%. The annual mean total cloud amount over the Arctic is 78% in CAM3 versus 74% in CCSM3. A complete description of CCSM3's cloud climatology, including its annual cycle of simulated cloud amount, is found in Vavrus and Waliser (2008).

As suggested by its realistic sea ice distribution, CCSM3 produces a reasonable present-day Arctic climatology compared with observations and is one of only two CMIP3 models with ice loss compatible with satellite-derived, late twentieth-century trends (Holland et al. 2006a). CCSM3's Arcticwide temperature bias is smaller than the CMIP3 average (Chapman and Walsh 2007), but the model generates a relatively wet climate poleward of 70°N compared with other GCMs and observations (Kattsov et al. 2007). The model's transient global climate response of 1.5 K is toward the low end of the range among CMIP3 models (Kiehl et al. 2006; Gregory and Forster 2008), but CCSM3 simulates one of the largest future Arctic temperature increases and sea ice decreases by the late twenty-first century (Chapman and Walsh 2007; Holland et al. 2008).

CCSM3's fidelity in its representation of sea ice and clouds is important for obtaining a credible simulation of future polar climates. GCMs tend to be more sensitive to greenhouse forcing when Arctic sea ice in their modern control runs is relatively thin and extensive (Rind et al. 1995; Holland and Bitz 2003). Likewise, models that incorrectly simulate more Arctic clouds during winter than summer in the present climate exhibit very little future cloud change (Vavrus et al. 2009).

c. Description of experiments

Four pairs of experiments are utilized in this study to assess the impact of local changes in sea ice cover and

TABLE 1. Description of the CAM3 simulations used in this study.

Expt	Mean SST	SST anomaly	Mean sea ice	Sea ice anomaly	CO_2 (ppm)
CONTROL	1950–2001 avg	None	1950–2001 avg	None	355
CAM_BOTH	1950–2001 avg	CCSM3 2 × CO_2 − CCSM3 control	1950–2001 avg	CCSM3 2 × CO_2 − CCSM3 control	355
CAM_SST	1950–2001 avg	CCSM3 2 × CO_2 − CCSM3 control	1950–2001 avg	None	355
CAM_ICE	1950–2001 avg	None	1950–2001 avg	CCSM3 2 × CO_2 − CCSM3 control	355

remote changes in SSTs on future Arctic cloudiness, as summarized below and in Table 1.

1) CCSM: The difference between the fully coupled CCSM3's modern control run and its transient 2 × CO_2 simulation.
2) CAM_BOTH: The difference between CAM3's modern control run (using observed sea ice concentration and SSTs) and its simulation with these boundary conditions added to the change in sea ice concentration and SSTs globally from the CCSM3 transient 2 × CO_2 simulation.
3) CAM_SST: Like CAM_BOTH, but only SSTs are altered from modern.
4) CAM_ICE: Like CAM_BOTH, but only sea ice concentration is altered from modern.

The surface boundary conditions of sea ice concentration and SSTs in the CAM3 control run are based on modern observations (1950–2001) (Collins et al. 2006b). In all CAM3 simulations, sea ice thickness is set to 2 m, and the temperature of any open-water regions coexisting with fractional ice cover is set to the freezing point of seawater (−1.8°C). In CAM3's greenhouse runs (CAM_BOTH, CAM_SST, and CAM_ICE), the observed sea ice concentrations and SSTs are added to their differences between a CCSM3 simulation forced with 2 × CO_2 and a CCSM3 modern control run (the delta method). CCSM3's control run is forced with the observed greenhouse gas concentration from year 1990 (355 ppm), and its future simulation represents a doubled CO_2 concentration based on a 1% yr^{-1} gain starting from year 1990. Because this rate of increase produces a doubling 70 years into the simulation, we use the average surface boundary conditions over the 20-year period straddling year 70 (years 61–80). A 20-year averaging period is also used to calculate climatological statistics (temperature, cloud amount, etc.) in all of the simulations. A five-year spinup interval preceded this averaging period in the CAM3 runs to allow the climate system to adjust fully to the altered boundary conditions.

In all CAM3 simulations the atmospheric greenhouse gas concentrations were fixed at their 1990 levels, following the approach of Higgins and Cassano (2009) and Deser et al. (2010), to isolate the role of changes in sea ice and SSTs. The differences in sea ice concentration and SSTs that represent CCSM3's response to the doubling of CO_2 are calculated from the coupled model's monthly mean values. Where sea ice (≥15% coverage) transitioned to open water in the CCSM3 greenhouse run, SSTs were set to the freezing point of seawater (−1.8°C), as were any open-water regions that coexisted with fractional ice cover in a grid box. Unlike Higgins and Cassano (2009) and Deser et al. (2010) but similar to Singarayer et al. (2006) and Seierstad and Bader (2009), we account for greenhouse-forced SST changes outside of ice-covered grid points as described above. Because the CO_2 increase in the CAM3 simulations is neglected, we expect that the atmospheric response to the imposed changes in sea ice and SSTs will be muted but qualitatively similar to that in the fully coupled 2 × CO_2 CCSM3 run. The response over land should be particularly weakened using this approach. We discuss the implications of this experimental design in section 4.

3. Results

a. General 2 × CO_2 response

The 2 × CO_2 changes in Arctic sea ice concentration and global SSTs are shown in Fig. 1. Northern Hemisphere sea ice area decreases annually by 27%, with the largest reductions occurring during late summer–early autumn, while the global-mean SST increases by 0.94 K. These changes are very similar to those occurring by the late twenty-first century in CCSM3's simulation using the conservative Special Report on Emissions Scenarios (SRES) B1 emissions scenario. The largest reductions in ice cover occur along the boundary between the Arctic Ocean and the northeastward extension of the North Atlantic Drift. In particular, a very pronounced loss of sea ice (over 40%) is apparent between Novaya Zemlya, Severnaya Zemlya, and the North Pole. Open-ocean surface waters warm almost everywhere, except for slight

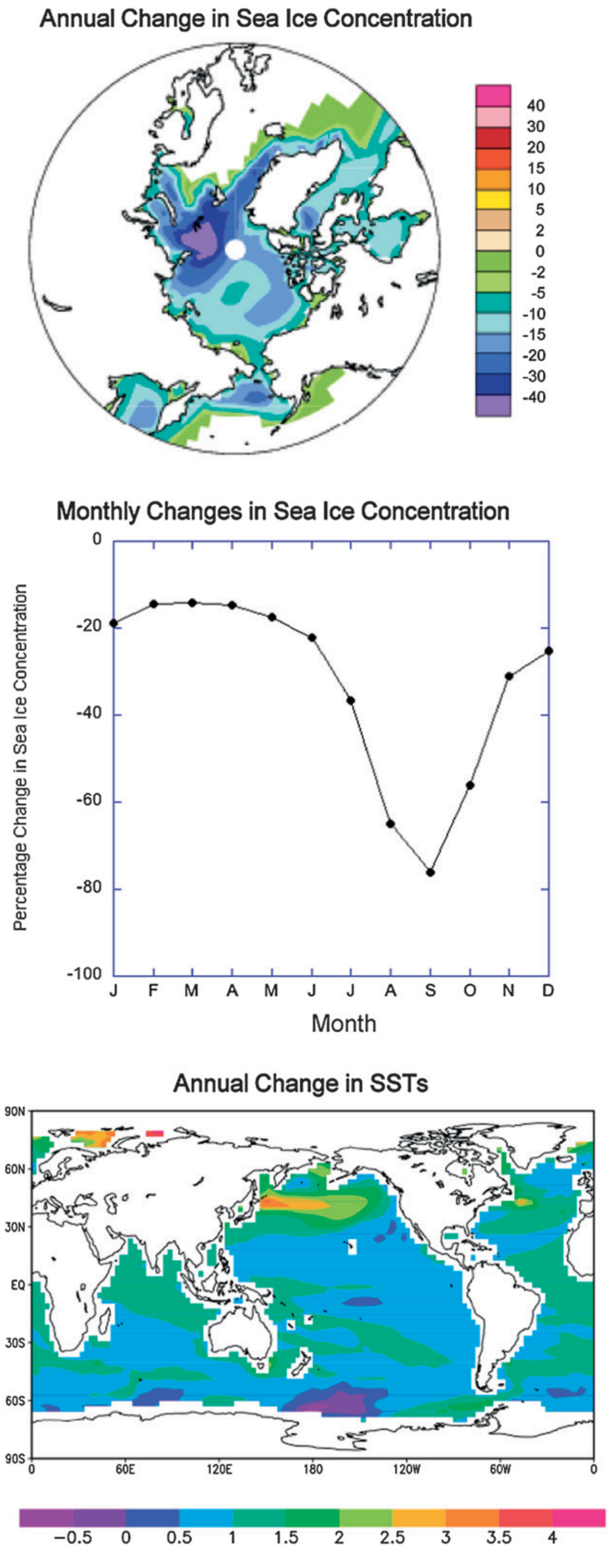

FIG. 1. Changes in average (top) annual and (middle) monthly Northern Hemisphere sea ice concentration (%) and (bottom) annual SSTs (K) at the time of CO_2 doubling in CCSM3. Values are 20-year annual averages.

cooling equatorward of the Ross Sea ice pack. SSTs across most of the Atlantic Ocean rise by 1–1.5 K, while changes in the Pacific vary more widely, ranging from no more than 1 K in much of the tropics and subtropics to 1.5–3.5 K in the North Pacific. Another region with enhanced surface warming is the Barents and Kara Seas (in excess of 2.5 K).

Associated with these warmer and less icy conditions are changes in cloudiness in most regions that vary with height. Under greenhouse forcing, CCSM3's global cloud response (not shown) is similar to that reported in Meehl et al. (2007) for the CMIP3 GCMs in the SRES A1B scenario—total cloud decreases in most of the world but increases in polar regions, especially the Arctic. Northern high latitudes exhibit a pronounced tripole pattern of cloud increases at low and high levels but little change in between (Fig. 2). CCSM3's transient 2 × CO_2 run generates a similar structure, but its cloud increases are greater at most heights. Likewise, the corresponding cloud distribution in CAM_BOTH resembles that of the fully coupled model but with a tempered response that is about 1% weaker at a given level than the cloud increases in CCSM3.

b. *Arctic cloud response spatially*

The general agreement between these three sets of output suggests that the Arctic cloud response is robust and that the mechanisms causing this spatially averaged polar cloud behavior may be similar. More detailed insight into the cloud response can be inferred from the spatial patterns of Arctic cloud changes among the four CCSM3–CAM3 experiments (Fig. 3). In CCSM3, changes in vertically integrated cloudiness are closely associated with sea ice cover, such that total cloud amount increases where pack ice exists at present but decreases over the perennially open-water regions in the Nordic and Barents Seas (Fig. 3a). A similar dipole pattern in the other CMIP3 GCMs was identified by Vavrus et al. (2009). This first-order response also appears in the CAM_BOTH simulation, although the cloud increases in that run are more accentuated in the eastern Arctic and the cloud decreases over adjacent open-water areas are more pronounced. A comparison of CAM_BOTH with the corresponding patterns in CAM_SST and CAM_ICE reveals that the total cloud response is almost entirely caused by the diminishing ice pack: the spatial distribution of cloud changes in CAM_ICE nearly matches that of CAM_BOTH (pattern correlation = 0.84), whereas there is no correlation between CAM_SST and CAM_BOTH ($r = -0.05$). Because low clouds are so prevalent in the Arctic, it is not surprising that the changes in total cloudiness bear a very strong resemblance to low cloud changes (Fig. 3b). Again, we

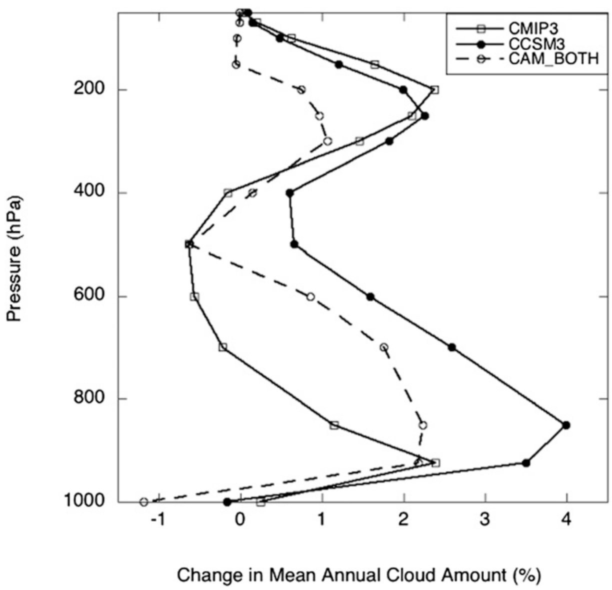

FIG. 2. Vertical cross section of the change in annual mean Arctic cloud amount (70°–90°N) at the time of CO_2 doubling in CCSM3 (solid line, solid circles) and CAM_BOTH (dashed line, open circles). Also shown is the multimodel mean response of the CMIP3 GCMs for the late twenty-first century minus the late twentieth century in the SRES A1B scenario (solid line, open squares).

see that the polar cloud changes are closely associated with reduced ice cover within the Arctic, rather than with increased SSTs outside the region.

The cloud changes at middle levels (700–400 hPa) show a very different and more complex pattern (Fig. 3c). The cloud response at these heights is relatively weak, but the changes are more positive in CCSM3 than in the CMIP3 average (Fig. 2). In the fully coupled CCSM3 simulation, middle clouds increase over most of the 60°–90° domain (76% of the area), with the largest gains centered over the Barents Sea, Bering Strait, and Canadian Archipelago and a smaller positive anomaly (<2%) over the rest of the Arctic Ocean. A somewhat similar pattern occurs in CAM_BOTH (middle clouds increase over 71% of the domain), although the local maximum near the Bering Strait is shifted to the southwest and there is no widespread positive anomaly over the Arctic Ocean. Unlike the case with total and low clouds, the midlevel cloud response is not dictated by changes in ice cover but appears to have contributions from both the reduced ice pack (CAM_ICE) and higher SSTs (CAM_SST). In particular, CCSM3's 4%–6% increase in middle cloud amount over the Barents Sea (2%–4% in CAM_BOTH) has roughly equal contributions from the changes in SSTs and sea ice. By contrast, most of the middle cloud gain over the Canadian Archipelago in CCSM3 and CAM_BOTH stem from the SST response. The primary signal over the Arctic ice pack in CAM_ICE is a small decrease in midlevel clouds. The overall pattern correlation with the changes in CCSM3's middle cloud amount poleward of 60° agrees better in CAM_SST than in CAM_ICE (r = 0.33 versus 0.19), as does the area covered by middle cloud gains (71% in CAM_SST versus 52% in CAM_ICE).

The high cloud response in CCSM3 (Fig. 3d) is a nearly ubiquitous increase throughout the Arctic (98% of the area poleward of 60°N), similar to the behavior of other CMIP3 models (Meehl et al. 2007; Vavrus et al. 2009). Although not quite as pronounced, the high cloud increases in CAM_BOTH are also very widespread (covering 86% of the region). This enhanced cloudiness at high levels is accounted for by the warmer global ocean and not by the reduced ice cover. CAM_SST produces high cloud increases over 96% of the 60°–90° domain—nearly the same as CCSM3—whereas high cloudiness mostly *declines* over this region in CAM_ICE (only 39% of the area shows a gain), especially above the Arctic Ocean.

c. *Arctic-average cloud response*

A summary of the Arctic-averaged cloud changes is presented in Fig. 4 for annual mean conditions and during the coldest (November–April) and warmest (May–October) half years. Although the maps of cloud changes were extended to 60°N to provide context, the areally averaged values in these graphs are calculated over the more traditional Arctic domain poleward of 70°N. This choice better captures the cloud response north of the major landmasses (whose surface boundary conditions were unchanged), is more consistent with the definition of the Arctic used in other studies (Nakamura and Oort 1988; Serreze et al. 1995), and allows a cleaner interface with the calculations of meridional moisture import described later. Annually averaged (Fig. 4a), Arcticwide cloud amount increases at all levels in CCSM3, ranging from 1.5% (low cloud) to 2.7% (high cloud). A similar type of cloud change occurs in CAM_BOTH, but the response is less pronounced (around one-third to one-half the magnitude of the fully coupled model). The contrasting influence on cloud changes from less sea ice and a warmer ocean is apparent in the area averages for CAM_SST and CAM_ICE. The loss of ice cover causes low clouds to become more abundant (CAM_ICE) by an amount equal to that with higher SSTs included (CAM_BOTH), although low clouds decrease in magnitude with higher SSTs alone (CAM_SST). Along the same lines, high cloudiness increases in CAM_SST—even exceeding the gain in CAM_BOTH—but decreases when forced

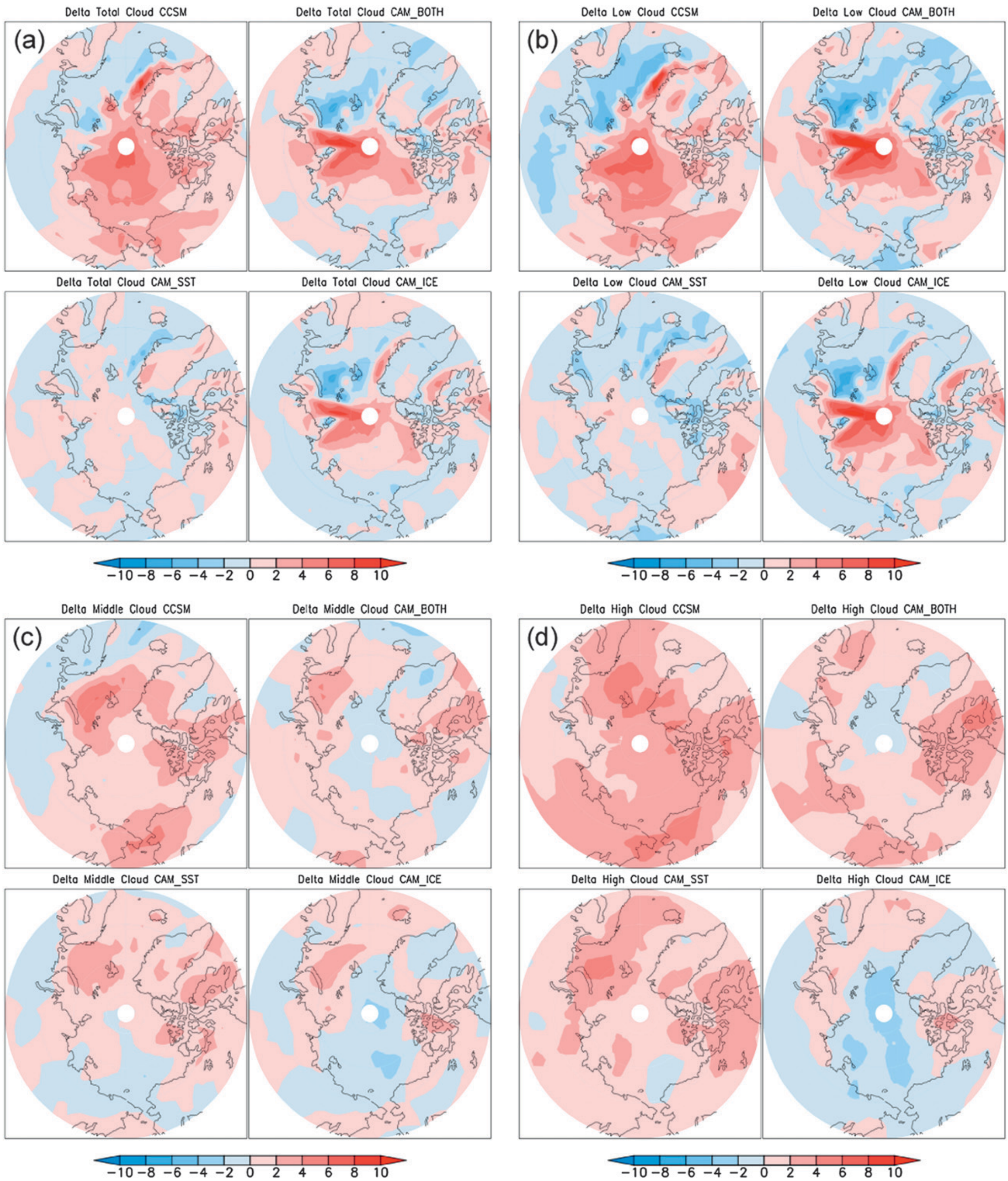

FIG. 3. Changes in mean annual Arctic cloud amount (%) at the time of CO_2 doubling in the four experiments: (a) total clouds, (b) low clouds, (c) middle clouds, and (d) high clouds.

with the sea ice retreat alone (CAM_ICE). Although midlevel clouds become more abundant in all simulations, they are much more responsive in CAM_SST (+1.0%) than in CAM_ICE (+0.1%).

Because polar clouds have very different radiative impacts during the course of the year, it is important to consider how the cloud changes vary by season among the experiments. In CCSM3 the largest cloud increases

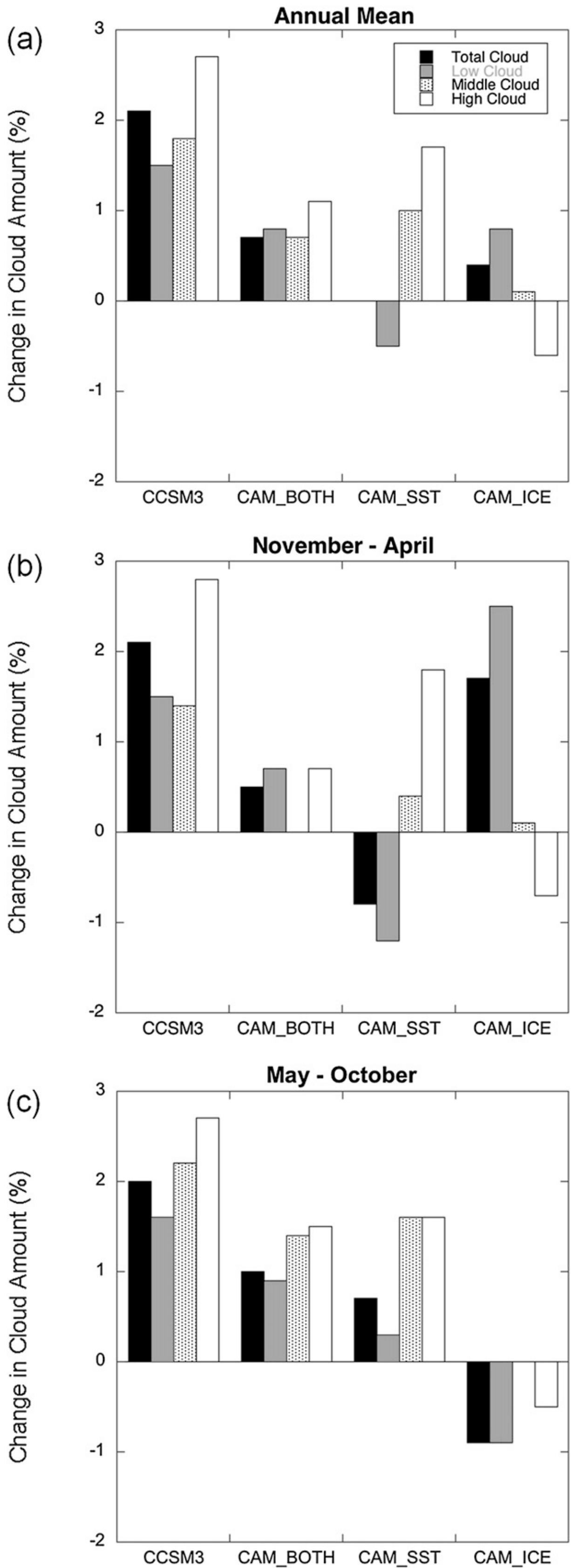

occur during autumn (3.9%), when the combination of more open water and an unstable boundary layer maximizes the rate of evaporation from the Arctic Ocean. During other seasons, the gain in cloudiness is much smaller and fairly uniform (1.3% in winter, 1.7% in spring, and 1.4% in summer). Although estimates differ as to the duration of summer when Arctic clouds impart a net cooling on the surface, there is agreement that cloud cover throughout autumn, winter, and spring acts as a warming mechanism (e.g., Schweiger and Key 1994). Accordingly, we compare the annual cloud changes with those occurring during the coldest half year (November–April) to infer whether the altered cloud amounts reinforce or mitigate the greenhouse warming signal (Fig. 4b). The changes in cloud amount during the coldest months strongly resemble annual-mean values in CCSM3, as well as in CAM_BOTH (except for middle clouds). This similarity extends to high cloud changes in CAM_SST and CAM_ICE. The most noticeable difference between the cold season and mean annual changes among the experiments is the response of low clouds and total clouds to the separate influences of modified sea ice and SST conditions. From November to April, low clouds decrease Arcticwide by more than 1% in CAM_SST (more than double the annual response), whereas they increase by 2.5% in CAM_ICE (triple the annual response). Consequently, the total cloud change during the coldest half year is negative in CAM_SST but is even more positive in CAM_ICE (1.7%) than the annual-mean change (0.4%). During the warmest half year (May–October), the changes in total and low cloudiness in CAM_SST and CAM_ICE flip sign from their cold half-year values (Fig. 4c). During May–October, total cloud cover increases by 0.7% in CAM_SST, primarily due to substantial increases in middle–high clouds but also a small gain in low clouds. Conversely, the amount of total and low cloudiness in CAM_ICE declines by 0.9% during this period, in sharp contrast with the larger increases during the colder months.

Although the magnitude of these cloud changes may seem small, they can have significant impacts on the Arctic energy budget. In particular, the difference in the change of low cloud cover during the coldest months

←

FIG. 4. Changes in areally averaged Arctic cloud amount (70°–90°N) among the four experiments at the time of CO_2 doubling for (a) annual mean, (b) November–April mean, and (c) May–October mean. (solid) Total clouds, (gray) low clouds, (stippled) middle clouds, and (open) high clouds.

TABLE 2. Changes in surface CRF (W m^{-2}) annually and during the colder half year using the modified formula in Vavrus (2006).

Expt	Change in CRF (annual)	Change in CRF (Nov–Apr)
CCSM3	−1.52	3.84
CAM_BOTH	−0.88	4.75
CAM_SST	−1.08	0.51
CAM_ICE	1.37	5.52

between CAM_ICE (positive) and CAM_SST (negative) translates into a very large difference in the coinciding surface CRF—an increase of 5.5 W m^{-2} caused by the sea ice reductions but only 0.5 W m^{-2} due to the warmer oceans (Table 2). This disparity occurs in spite of high clouds increasing during November–April in CAM_SST but decreasing in CAM_ICE. The large positive change in CRF during the cold half year in CAM_ICE is big enough to cause an increase in the annual mean CRF in that simulation (1.4 W m^{-2}), whereas all the other experiments produce a CRF decline when averaged throughout the year. Thus, the loss of sea ice initiates a very pronounced gain in low cloudiness when clouds are most effective at trapping heat, and this cold-season response is large enough to dictate the sign of the annual mean CRF change. Interpreting the role of cloud changes on surface heating during the warm half year is much more difficult. In the present-day climate system, the effect of clouds during this period varies between surface warming (May, September, and October) and cooling (June–August) (Schweiger and Key 1994), therefore a time-mean change in cloudiness averaged over this period could favor either a warmer or cooler surface. Even breaking down the changes in time-mean cloud amount by month is problematic because the magnitude and even the sign of summertime changes in CRF are often dictated by the surface albedo response as the ice pack wanes, rather than by cloud changes. We therefore focus on the more straightforward interpretation of the radiative impacts of cloud changes during the coldest half year.

d. *Possible mechanisms*

The strikingly different changes in low clouds versus middle–high clouds between CAM_ICE and CAM_SST suggest that more than one physical mechanism is responsible for the Arctic cloud increases simulated by CCSM3. Because projected total cloud increases in the Arctic are significantly correlated with enhanced evaporation locally (Vavrus et al. 2009) and because the spatial pattern of the low cloud changes in these experiments is highly correlated with total cloud changes (Fig. 3a), increased evaporation due to less ice cover is a plausible explanation for the simulated increase in low clouds. The patterns of latent heat flux changes (Fig. 5) support this hypothesis, showing widespread increases in evaporation over the most of the Arctic that generally correspond to the spatial distribution of low cloud changes over polar oceans (Fig. 3b). The localized peak increase in evaporation between Franz Josef Land and Severnaya Zemlya in all but the CAM_SST simulation must be a consequence of the collocated maximum decline in sea ice (Fig. 1) and appears to explain the peak gain in low cloudiness over this region in CAM_BOTH and CAM_ICE. The latent heat response in CAM_SST is completely different, however, featuring slight decreases throughout the Arctic Ocean that are consistent with the near absence of low cloud increases over the ice pack. Outside of the sea ice regime, the latent heat flux response is opposite between CAM_SST and CAM_ICE—where warmer waters are allowed in the Nordic–Barents Seas there is much more evaporation (CAM_SST), compared with the slightly decreased evaporation in these areas in CAM_ICE.

Despite these differences in latent heat flux changes in this region, all simulations produce more middle and high clouds over the Barents Sea (Fig. 3). CCSM3 is most pronounced in this regard, simulating a maximum in the vicinity of Spitsbergen (and another around the Bering Strait). These localized increases in mid–high-level cloudiness appear to be regulated not by surface forcing but by vertically integrated moisture transport. Within two boxes that encompass the largest such cloud increases in CCSM3—74°–78°N, 0°–50°E (Spitsbergen) and 64°–67°N, 178°E–152°W (Bering Strait)—we find that the monthly changes in combined middle and high cloudiness are correlated with the monthly changes in meridional moisture flux convergence at $r = 0.59$ and 0.81, respectively, both of which are statistically significant at the 95% confidence level.

In fact, a likely explanation for the *Arcticwide* middle and high cloud increases is the enhanced poleward moisture transport that typically accompanies simulated greenhouse warming due to a moister global atmosphere (e.g., Manabe and Wetherald 1975; Held and Soden 2000). In keeping with the usual Arctic boundary of 70°N in calculations of polar energy import (Overland et al. 1996; Semmler et al. 2005), we computed the meridional moisture influx throughout the troposphere in all four experiments to illustrate how this quantity changes (Fig. 6). The moisture transport (Vq) to the Arctic increases throughout the troposphere in the simulations with higher SSTs but decreases at all levels without this change (CAM_ICE). Also apparent in the three runs with ocean warming is the general percentage increase in Vq with height above 700–900 hPa that is

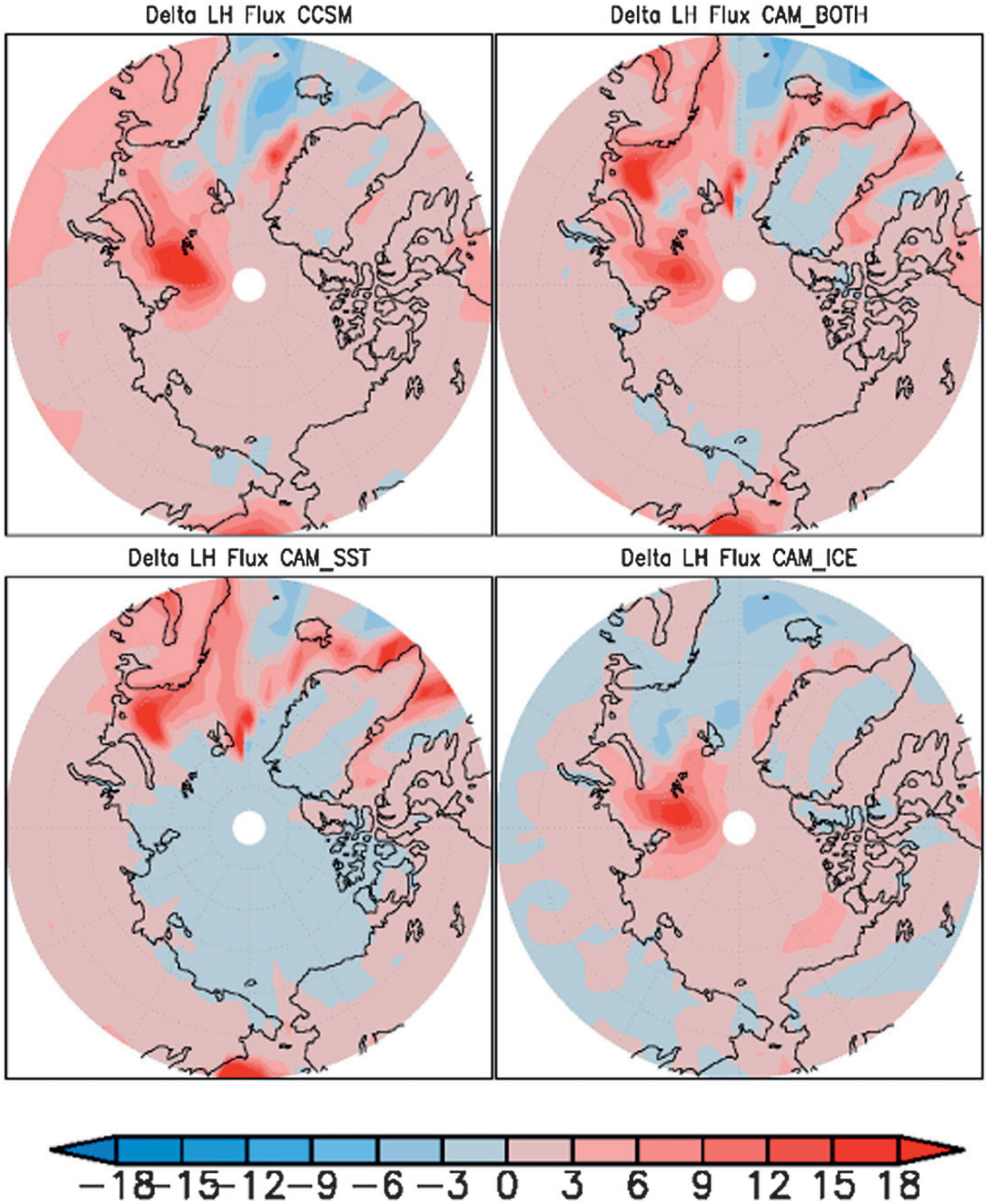

FIG. 5. Change in mean annual latent heat flux (W m^{-2}) at the time of CO_2 doubling in the four experiments.

indicative of enhanced moisture transport by eddies above the boundary layer, similar to the process responsible for the observed peak in Arctic high clouds during winter (Eastman and Warren 2010b).

These results provide support for the notion that low cloud changes are mostly linked to local evaporation, while the response of middle and high clouds is primarily attributable to remotely triggered moisture transport aloft. As further evidence, we show the relationship between the change in Arctic-averaged cloud amounts (total, low, middle, and high) and the changes in meridional moisture import and local evaporation (Fig. 7). When linearly correlated across the four experiments, these annually averaged quantities demonstrate a clear distinction between the two hypothesized forcing mechanisms. The increase in total and low clouds is very closely tied to the local increase in evaporation within the Arctic (r = 0.82 and 0.93, respectively) but only weakly (or inversely) related to the remotely driven gain in moisture transport. By contrast, the increase in middle

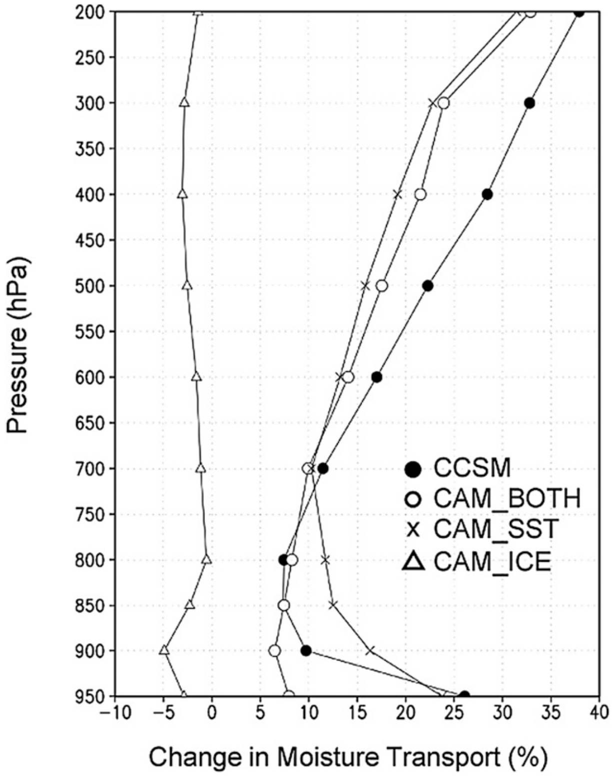

FIG. 6. Vertical cross section of the percentage change in meridional moisture transport into the Arctic (70°N) at the time of CO_2 doubling among the four experiments. (solid circles) CCSM3, (open circles) CAM_BOTH, (crisscrosses) CAM_SST, and (open triangles) CAM_ICE.

and high clouds is very highly correlated with the increase in moisture import ($r = 0.82$ and 0.92, respectively) but much less related to the local enhancement of surface moisture fluxes. This breakdown thus seems to provide the physical basis for the simulated cloud changes with height in CCSM3, whose response resembles the typical behavior of other state-of-the-art GCMs in CMIP3.

4. Discussion and conclusions

This study demonstrates the variable nature of projected future Arctic cloud changes. Not only is the cloud response a strong function of height but so too are the associated mechanisms. Although the CAM_BOTH simulation serves as an approximation of the fully coupled CCSM3 run, we recognize that its response is muted. This curtailed sensitivity could be caused by many factors, but certainly a big reason is the absence of explicit greenhouse warming over land in CAM_BOTH. Other possible factors include the neglect of high-frequency (daily) variability of sea ice cover and SSTs, as well as the constant 2-m sea ice thickness prescribed in the CAM3 runs compared with the variable ice thickness distribution in CCSM3 (Holland et al. 2006b) that was used by Deser et al. (2010) and Higgins and Cassano (2009). Also, this study only considers changes in cloud *amount*, even though related properties such as water vapor and cloud phase also exert a strong influence on the Arctic radiation budget (Gorodetskaya et al. 2008). In addition, we did not explicitly address the potential influence of changes in specific circulation patterns, following the conclusion in Vavrus et al. (2009) that the Arctic cloud changes in the CMIP3 models were not significantly correlated with changes in sea level pressure (SLP) in any season. However, dynamical influences that alter the meridional transport of moisture into the Arctic are identified here as a key factor in explaining the response of middle and high clouds. Furthermore, some of the mismatch in the regional patterns of cloud changes (Fig. 3) between CAM_BOTH and CCSM3 and between CAM_BOTH and its components, CAM_ICE and CAM_SST, can be explained by differences in internal dynamical variability within each simulation. These smaller-scale discrepancies are reduced when we consider areally averaged quantities, such as those in Fig. 4.

Despite these caveats, the major features of changes in polar clouds and moisture fluxes (both vertical and horizontal) in CCSM3 are captured by CAM_BOTH, whose response can be decomposed into the sea ice–forced and SST-forced components. This technique illustrates that projected cloud changes in the Arctic are caused by both local and remote factors and that these two drivers are nearly orthogonal to each other between low atmospheric levels and middle-high levels. Locally, enhanced evaporation in the Arctic—particularly within the eroding ice pack—drives increases in low clouds and explains why the pattern of enhanced low cloudiness overlaps so closely with that of sea ice cover. Remotely, the more moisture-laden global atmosphere leads to a stronger meridional moisture flux into the Arctic—especially above the boundary layer—and thus greater cloudiness at middle and high levels. This finding is similar to the one reported by Higgins and Cassano (2009), who showed that the projected increase in wintertime Arctic precipitation is driven by enhanced meridional water vapor transport stemming from a much moister atmosphere. Similarly, Alexeev et al. (2005) found that greater poleward moisture flux under greenhouse warming is a major reason for polar amplification.

Although the simulated Arctic cloud changes are consistent with this interpretation, we cannot preclude other relevant mechanisms from playing a role. First, one might expect that a moister atmosphere in a greenhouse-warmed world would necessarily lead to a cloudier

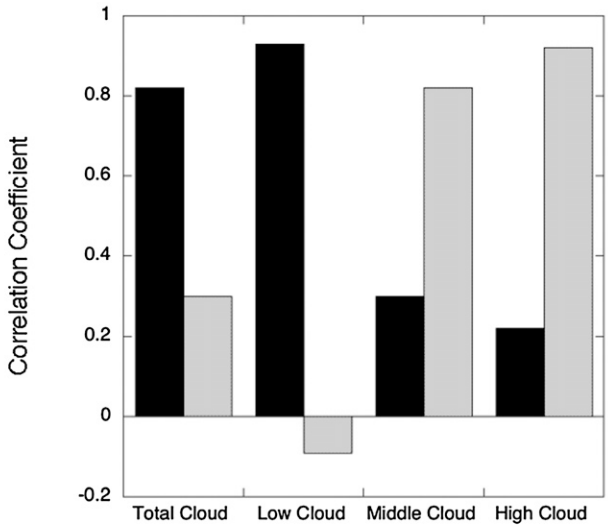

FIG. 7. Correlation of changes in Arctic cloud amount vs changes in local evaporation (black) and changes in remote moisture transport into the Arctic (gray) across the four experiments. All values denote correlations of mean-annual conditions over the domain 70°–90°N.

Arctic, but about one-third of GCMs in the CMIP3 collection simulated very little future cloud increase (those with a distorted annual cycle of present-day Arctic cloudiness) and an early version of the CCSM simulated considerably fewer low and middle clouds in polar regions (Vavrus et al. 2009, Dai et al. 2001). Thus, because a warmer Arctic atmosphere has a higher moisture-holding capacity, a moister climate will not necessarily lead to more clouds. Second, the high cloud increases in polar regions identified in early 2 $\times$ CO_2 modeling studies (Wetherald and Manabe 1986; Wilson and Mitchell 1987) were attributed to an inflated tropopause height that enhanced high cloudiness globally. This explanation is not inconsistent with the role of strengthened meridional moisture transport that we associate with CCSM3's high cloud gain in the Arctic because the increase in specific humidity aloft is most pronounced in the source region at lower latitudes. Third, although Schweiger et al. (2008) found evidence for reduced low clouds and enhanced middle clouds where sea ice losses occur (due to weakened atmospheric stability), that study was focused on the response at the ice margin and within the context of present-day interannual variability. Finally, Beesley and Moritz (1999) hypothesized that the abundance of Arctic low clouds is highly temperature-dependent owing to ice microphysical properties and therefore the region is cloudier during summer, when cloud phase is predominantly liquid. Their reasoning supports an expectation that the Arctic would become cloudier in a warmer mean climate (at least in the lower troposphere), consistent with our findings. Their explanation for the existence of low Arctic clouds could complement our emphasis on evaporation within the ice pack because more of the longer-lived liquid cloud condensate would arise from enhanced evaporation amid reduced ice cover.

The most radiatively important feedback loop suggested by these simulations operates during the coldest months—less ice cover causes more low clouds that trap surface energy emission and in turn favor less (or thinner) sea ice. Recent evidence from satellite measurements and surface observations supports the simulated inverse relationship between low clouds and ice cover, especially during autumn (Kay and Gettelman 2009; Eastman and Warren 2010a; Palm et al. 2010). We find that convective clouds do not play a significant role in explaining the enhanced cloudiness at middle and high levels in these simulations, consistent with the requirement for stronger greenhouse forcing (4 x CO_2) needed to initiate convection in CCSM3 (Abbot and Tziperman 2008).

Although these conclusions may be model dependent, CCSM3's Arctic cloud response to greenhouse warming has been shown to be representative of other state-of-the-art GCMs used in CMIP3. Thus, our diagnosis of the underlying physical mechanisms may apply to other climate models that simulate increased future cloudiness in this region. The simulated Arctic climate change and cloud response in CCSM3 is similar between the T42 horizontal resolution used in this study and the model's standard T85 resolution. A new version of the model (CCSM4) has recently been released and shows a similar tripole vertical cloud response, despite a new parameterization for low cloud concentration in polar regions (Vavrus and Waliser 2008).

Acknowledgments. This work has been supported by the National Science Foundation (OPP-0327664, ARC-0628910, and ARC-0652838) and by the Japan Agency for Marine-Earth Science and Technology (JAMSTEC). We thank the National Center for Atmospheric Research, which is sponsored by the National Science Foundation, for the computing time used in this research.

REFERENCES

Abbot, D. S., and E. Tziperman, 2008: A high-latitude convective cloud feedback and equable climates. *Quart. J. Roy. Meteor. Soc.,* **134,** 165–185, doi:10.1002/qj.211.

Alexander, M. A., U. S. Bhatt, J. E. Walsh, M. S. Timlin, J. S. Miller, and J. D. Scott, 2004: The atmospheric response to realistic Arctic sea ice anomalies in an AGCM during winter. *J. Climate,* **17,** 890–905.

Alexeev, V. A., and J. A. Bates, 1999: GCM experiments to test a proposed stabilizing mechanism in the climate system. *Tellus,* **51A,** 630–651.

——, P. L. Langen, and J. R. Bates, 2005: Polar amplification of surface warming on an aquaplanet in ''ghost forcing'' experiments without sea ice feedbacks. *Climate Dyn.,* **24,** 655–666, doi:10.1007/s00382-005-0018-3.

Beesley, J. A., and R. E. Moritz, 1999: Toward an explanation of the annual cycle of cloudiness over the Arctic Ocean. *J. Climate,* **12,** 395–415.

Bekryaev, R. V., I. V. Polyakov, and V. A. Alexeev, 2010: Role of polar amplification in long-term surface air temperature variations and modern arctic warming. *J. Climate,* **23,** 3888–3906.

Bhatt, U. S., M. A. Alexander, C. Deser, J. E. Walsh, J. S. Miller, M. Timlin, J. D. Scott, and R. Tomas, 2008: The atmospheric response to realistic reduced summer Arctic sea ice anomalies. *Arctic Sea Ice Decline: Observations, Projections, Mechanisms, and Implications, Geophys. Monogr.,* Vol. 180, Amer. Geophys. Union, 91–110.

Bitz, C. M., and W. H. Lipscomb, 1999: An energy-conserving thermodynamic model of sea ice. *J. Geophys. Res.,* **104,** 15 669–15 677.

Bonan, G. B., K. W. Oleson, M. Vertenstein, S. Levis, X. Zeng, Y. Dai, R. E. Dickinson, and Z.-L. Yang, 2002: The land surface climatology of the Community Land Model coupled to the NCAR Community Climate Model. *J. Climate,* **15,** 3123–3149.

Boville, B. A., P. J. Rasch, J. J. Hack, and J. R. McCaa, 2006: Representation of clouds and precipitation processes in the Community Atmosphere Model (CAM3). *J. Climate,* **19,** 2184–2198.

Briegleb, B. P., C. M. Bitz, E. C. Hunke, W. H. Lipscomb, M. M. Holland, J. L. Schramm, and R. E. Moritz, 2004: Scientific description of the sea ice component of the Community Climate System Model, version three. National Center for Atmospheric Research Tech. Rep. NCAR/TN-463+STR, 78 pp.

Chapman, W. L., and J. E. Walsh, 2007: Simulations of Arctic temperature and pressure by global coupled models. *J. Climate,* **20,** 609–632.

Collins, W. D., 2001: Parameterization of generalized cloud overlap for radiative calculations in general circulation models. *J. Atmos. Sci.,* **58,** 3224–3242.

——, and Coauthors, 2006a: The Community Climate System Model: CCSM3. *J. Climate,* **19,** 2122–2143.

——, and Coauthors, 2006b: The formulation and atmospheric simulation of the Community Atmospheric Model version 3 (CAM3). *J. Climate,* **19,** 2144–2161.

Comiso, J. C., 2003: Warming trends in the Arctic from clear-sky satellite observations. *J. Climate,* **16,** 3498–3510.

Cubasch, U., J. Waszkewitz, G. Hegerl, and J. Perlwitz, 1995: Regional climate changes as simulated in time-slice experiments. *Climatic Change,* **31,** 273–304.

Dai, A., T. M. L. Wigley, B. A. Boville, J. T. Kiehl, and L. E. Buja, 2001: Climates of the twentieth and twenty-first centuries simulated by the NCAR Climate System Model. *J. Climate,* **14,** 485–519.

Deser, C., R. Tomas, M. Alexander, and D. Lawrence, 2010: The seasonal atmospheric response to projected Arctic sea ice loss in the late twenty-first century. *J. Climate,* **23,** 333–351.

Eastman, R., and S. G. Warren, 2010a: Interannual variations of Arctic cloud types in relation to sea ice. *J. Climate,* **23,** 4216–4232.

——, and ——, 2010b: Arctic cloud changes from surface and satellite observations. *J. Climate,* **23,** 4233–4242.

Gent, P. R., and J. C. McWilliams, 1990: Isopycnal mixing in ocean circulation models. *J. Phys. Oceanogr.,* **20,** 150–155.

Gorodetskaya, I. V., L.-B. Tremblay, B. Liepert, M. A. Cane, and R. I. Cullather, 2008: Modification of the Arctic Ocean shortwave radiation budget due to cloud and sea ice properties in coupled models and observations. *J. Climate,* **21,** 866–882.

Graversen, R. G., and M. Wang, 2009: Polar amplification in a coupled climate model with locked albedo. *Climate Dyn.,* **33,** 629–643.

Gregory, J. M., and P. M. Forster, 2008: Transient climate response estimated from radiative forcing and observed temperature change. *J. Geophys. Res.,* **113,** D23105, doi:10.1029/2008JD010405.

Hack, J. J., 1994: Parameterization of moist convection in the NCAR Community Climate Model, CCM2. *J. Geophys. Res.,* **99** (D3), 5551–5568.

Hegseth, E. N., and A. Sundfjord, 2008: Intrusion and blooming of Atlantic phytoplankton species in the high Arctic. *J. Mar. Syst.,* **74,** 108–119.

Held, I. M., and B. J. Soden, 2000: Water vapor feedback and global warming. *Annu. Rev. Energy Environ.,* **25,** 441–475.

Higgins, M. E., and J. J. Cassano, 2009: Impacts of reduced sea ice on winter Arctic atmospheric circulation, precipitaion, and temperature. *J. Geophys. Res.,* **114,** D16107, doi:10.1029/2009JD011884.

Holland, M. M., and C. M. Bitz, 2003: Polar amplification of climate change in the coupled model intercomparison project. *Climate Dyn.,* **21,** 221–232.

——, ——, and B. Tremblay, 2006a: Future abrupt reductions in the summer Arctic sea ice. *Geophys. Res. Lett.,* **33,** L23503, doi:10.1029/2006GL028024.

——, ——, E. C. Hunke, W. H. Lipscomb, and J. L. Schramm, 2006b: Influence of the sea ice thickness distribution on polar climate in CCSM3. *J. Climate,* **19,** 2398–2414.

——, M. C. Serreze, and J. Stroeve, 2008: The sea ice mass budget of the Arctic and its future change as simulated by coupled climate models. *Climate Dyn.,* **34,** 185–200, doi:10.1007/s00382-008-0493-4.

Hunke, E. C., and J. K. Dukowicz, 1997: An elastic–viscous–plastic model for sea ice dynamics. *J. Phys. Oceanogr.,* **27,** 1849–1867.

Karlsson, J., and G. Svensson, 2009: The simulation of Arctic clouds and their influence on the winter surface temperature in present-day climate in the CMIP3 multi-model dataset. *Climate Dyn.,* **36,** 623–635, doi:10.1007/s00382-010-0758-6.

Kattsov, V. M., J. E. Walsh, W. L. Chapman, V. A. Govorkova, and T. V. Pavlova, 2007: Simulation and projection of Arctic freshwater budget components by the IPCC AR4 global climate models. *J. Hydrometeor.,* **8,** 571–589.

Kay, J. E., and A. Gettelman, 2009: Cloud influence on and response to seasonal Arctic sea ice loss. *J. Geophys. Res.,* **114,** D18204, doi:10.1029/2009JD011773.

Kiehl, J. T., C. A. Shields, J. J. Hack, and W. Collins, 2006: The climate sensitivity of the Community Climate System Model: CCSM3. *J. Climate,* **19,** 2584–2596.

Langen, P. L., and V. A. Alexeev, 2004: Multiple equilibria and asymmetric climates in the CCM3 coupled to an oceanic mixed layer with thermodynamic sea ice. *Geophys. Res. Lett.,* **31,** L04201, doi:10.1029/2003GL019039.

——, and ——, 2007: Polar amplification as a preferred response in an aquaplanet GCM. *Climate Dyn.,* **23,** 305–317.

Lawrence, D. M., A. G. Slater, R. A. Tomas, M. M. Holland, and C. Deser, 2008: Accelerated Arctic land warming and permafrost degradation during rapid sea ice loss. *Geophys. Res. Lett.,* **35,** L11506, doi:10.1029/2008GL033985.

Liu, Y., J. R. Key, and X. Wang, 2009: Influence of changes in sea ice concentration and cloud cover on recent Arctic surface temperature trends. *Geophys. Res. Lett.,* **36,** L20710, doi:10.1029/2009GL040708.

Manabe, S., and R. T. Wetherald, 1975: The effects of doubling the CO_2 concentration on the climate of a general circulation model. *J. Atmos. Sci.,* **32,** 3–15.

Meehl, G. A., and Coauthors, 2007: Global climate projections. *Climate Change 2007: The Physical Science Basis,* S. Solomon et al., Eds., Cambridge University Press, 747–845.

Miao, Q., and Z. Wang, 2008: Comparison on cloud and radiation properties at Barrow between ARM/NSA measurements and GCM outputs. *Proc. 18th Atmospheric Radiation Measurement (ARM) Science Team Meeting,* Norfolk, VA, ARM. [Available online at http://www.arm.gov/publications/proceedings/conf18.]

Nakamura, N., and A. H. Oort, 1988: Atmospheric heat budgets of the polar regions. *J. Geophys. Res.,* **93,** 9510–9524.

Overland, J. E., P. Turet, and A. H. Oort, 1996: Regional variations of moist static energy flux into the Arctic. *J. Climate,* **9,** 54–65.

——, M. Wang, and S. Salo, 2008: The recent Arctic warm period. *Tellus,* **60A,** 589–597.

Palm, S. P., S. T. Strey, J. Spinhirne, and T. Markus, 2010: The influence of Arctic sea ice extent on polar cloud fraction and vertical structure and implications for regional climate. *J. Geophys. Res.,* **115,** D21209, doi:10.1029/2010JD013900.

Rind, D., R. Healy, C. Parkinson, and D. Martinson, 1995: The role of sea ice in $2 \times CO_2$ climate model sensitivity. Part I: The total role influence of sea ice thickness and extent. *J. Climate,* **8,** 449–463.

Schweiger, A. J., 2004: Changes in seasonal cloud cover over the Arctic seas from satellite and surface observations. *Geophys. Res. Lett.,* **31,** L12207, doi:10.1029/2004GL020067.

——, and J. Key, 1994: Arctic Ocean radiative fluxes and cloud forcing estimated from the ISCCP C2 cloud data set, 1983–90. *J. Appl. Meteor.,* **33,** 948–963.

——, R. Lindsay, S. Vavrus, and J. Francis, 2008: Relationships between Arctic sea ice and clouds during autumn. *J. Climate,* **21,** 4799–4810.

Seierstad, I. A., and J. Bader, 2009: Impact of a projected future Arctic sea ice reduction on extratropical storminess and the NAO. *Climate Dyn.,* **33,** 937–943.

Semmler, T., D. Jacob, K. H. Schlünzen, and R. Podzun, 2005: The water and energy budget of the Arctic atmosphere. *J. Climate,* **18,** 2515–2530.

Serreze, M. C., R. G. Barry, and J. E. Walsh, 1995: Atmospheric water vapor characteristics at 70°N. *J. Climate,* **8,** 719–731.

Singarayer, J. S., J. L. Bamber, and P. J. Valdes, 2006: Twenty-first-century climate impacts from a declining Arctic sea ice cover. *J. Climate,* **19,** 1109–1125.

Smith, R., and P. Gent, 2004: Reference manual for the Parallel Ocean Program (POP) ocean component of the Community Climate System Model (CCSM2.0 and 3.0). Los Alamos National Laboratory Rep. LAUR-02-2484, 75 pp.

Stroeve, J., M. M. Holland, W. Meier, T. Scambos, and M. Serreze, 2007: Arctic sea ice decline: Faster than forecast. *Geophys. Res. Lett.,* **34,** L09501, doi:10.1029/2007GL029703.

Timbal, B., J.-F. Mahfouf, J.-F. Royer, U. Cubasch, and J. M. Murphy, 1997: Comparison between doubled CO_2 time-slice and coupled experiments. *J. Climate,* **10,** 1463–1469.

Vavrus, S., 2004: The impact of cloud feedbacks on Arctic climate under greenhouse forcing. *J. Climate,* **17,** 603–615.

——, 2006: An alternative method to calculate cloud radiative forcing: Implications for quantifying cloud feedbacks. *Geophys. Res. Lett.,* **33,** L01805, doi:10.1029/2005GL024723.

——, and D. Waliser, 2008: An improved parameterization for simulating Arctic cloud amount in the CCSM3 climate model. *J. Climate,* **21,** 5673–5687.

——, ——, A. Schweiger, and J. Francis, 2009: Simulations of 20th and 21st century Arctic clouds in the global climate models assessed in the IPCC AR4. *Climate Dyn.,* **33,** 1099–1115.

——, M. M. Holland, and D. A. Bailey, 2011: Changes in Arctic clouds during intervals of rapid sea ice loss. *Climate Dyn.,* **36,** 1475–1489.

Walsh, J. E., and Coauthors, 2005: Cryosphere and hydrology. *Arctic Climate Impact Assessment,* Cambridge University Press, 184–242.

——, D. H. Portis, and W. L. Chapman, 2008: Use of ARM/NSA products to evaluate IPCC-AR4 Arctic cloud and radiative simulations. *Proc. 18th Atmospheric Radiation Measurement (ARM) Science Team Meeting,* Norfolk, VA, ARM. [Available online at http://www.arm.gov/publications/proceedings/conf18/poster/P00076.pdf.]

Wang, X., and J. R. Key, 2003: Recent trends in Arctic surface, cloud, and radiation properties from space. *Science,* **299,** 1725–1728.

Wetherald, R. T., and S. Manabe, 1986: An investigation of cloud cover change in response to thermal forcing. *Climatic Change,* **8,** 5–24.

Wilson, C. A., and J. F. B. Mitchell, 1987: A doubled CO_2 climate sensitivity experiment with a GCM including a simple ocean. *J. Geophys. Res.,* **92,** 13 315–13 343.

Zhang, G. J., and N. A. McFarlane, 1995: Sensitivity of climate simulations to the parameterization of cumulus convection in the Canadian Climate Centre general circulation model. *Atmos.–Ocean,* **33,** 407–446.